Eidgenössische Technische Hochschule Zürich
Swiss Federal Institute of Technology Zurich

SED
Schweizerischer Erdbebendienst
Swiss Seismological Service

Report on site characterization

Emmethof, Switzerland (EMMET)

Poggi Valerio, Donat Fäh

Last modified - 22 / 12 / 2014

1. Introduction

In the framework of the NAGRA seismic network project, an array measurement of the ambient vibration wave-field was performed at the location of the SED station EMMET (Emmethof, Switzerland). The scope of the survey is the seismic characterization of the area surrounding the installation (**Figure 1**), which consists in a broadband seismometer (Trillium Compact) with a high-resolution digitizer (Taurus 24Bit @200sps). Ambient vibration analysis has been used to infer the characteristics of the underground structure of the site, with special regard to the one-dimensional shear-wave velocity. Such profile was later used to assess the local seismic response of the station.

For the analysis, different spectral analysis techniques were implemented, consisting in both single and array methods, which are listed below:

- Time-frequency wavelet analysis
- Power-spectral density estimation
- Conventional horizontal to vertical spectral ratios
- Directional horizontal to vertical spectral ratios
- Wavelet polarization analysis
- Three-component high-resolution f-k analysis.

The results of all these analyses conformed to the definition of the final velocity model. In the following, the main results of these investigations are summarized and a final interpretation of the velocity profile is given. From this interpretation, engineering parameters are finally derived, e.g. the Qwl-Vs average velocity, VsZ (including Vs30) and the seismic amplification from the analytical SH-transfer function of the one-dimensional soil column.

2. Survey description

To characterize the seismic response of the site, an array measurement of ambient vibration was performed on 09/10/2014 (**Figure 1**). The array consists of two concentric measuring configurations (called “rings”, R1 and R2) of 12 sensors each and increasing diameter (about 20m and 40m respectively). Three configurations were initially planned, together with a larger configuration of about 100m, but dense vegetation and steep slopes toward north and south limited the available space. Ring 1 and 2 were partially overlapping, with the aim of providing a continuous frequency resolution between the geometries. Configuration R1 recorded for a total of 1h, while configuration R2 for 1h and 30m. The differences in the recording length are due to the different resolution characteristics of the three geometries. As a general rule, larger arrays require longer recording time to produce a reasonable statistics of the ambient vibration processing results. Satisfactory results were obtained from the analysis of the first geometry only, while the second did not produced usable results. A limited penetration depth of about ~50-80m was initially expected, increased by the use of ellipticity information.

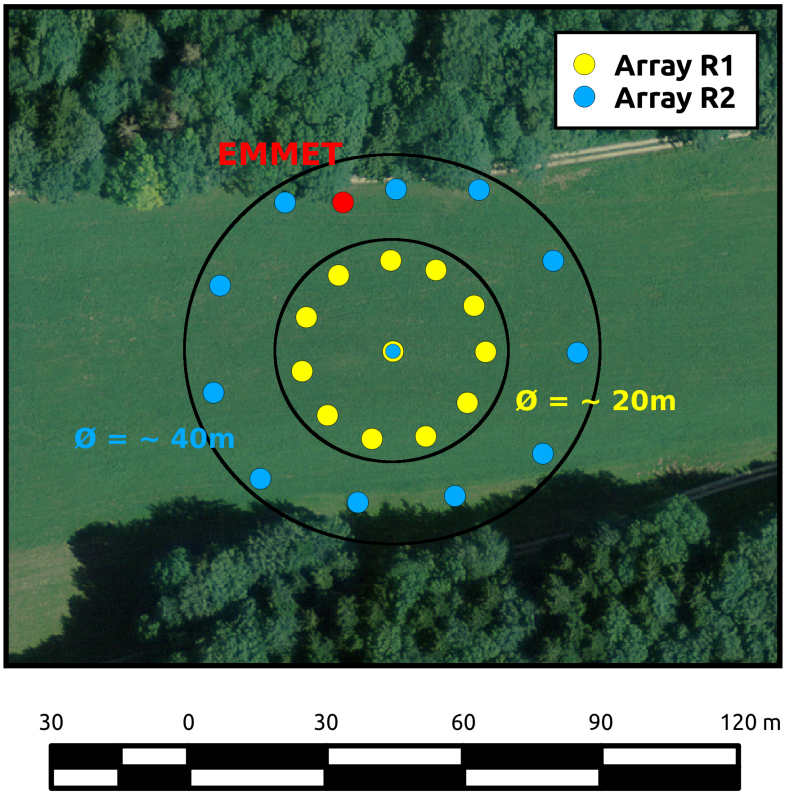

Figure 1 - *Location of the ambient vibration array survey performed in Emmethof (SED station EMMET) on 09/10/2014. Two concentric configurations of increasing diameter were implemented (named R1 and R2).*

3. Weather conditions

The weather conditions were optimal during the whole measurement, with no precipitations and an average temperature of 26 degrees.

4. Soil type, topography and geology

The array has been set in open field conditions, in a rural area (**Figure 1**, **Figure 3**). The influence of buildings and anthropogenic disturbances is virtually negligible. Array sensors have been deployed on free soil. Good coupling with the ground was assured by means of digging small holes at the sensor's places, and by using a special support (*Trihedron*®) that facilitates the leveling of the device even for difficult soil conditions. The measurement area was located on a gentle slope toward north; however no topographic correction was necessary before processing. Soil was mostly dry, with the exception of a limited zone at the southern edge of the array, which showed some evidence of water saturation.

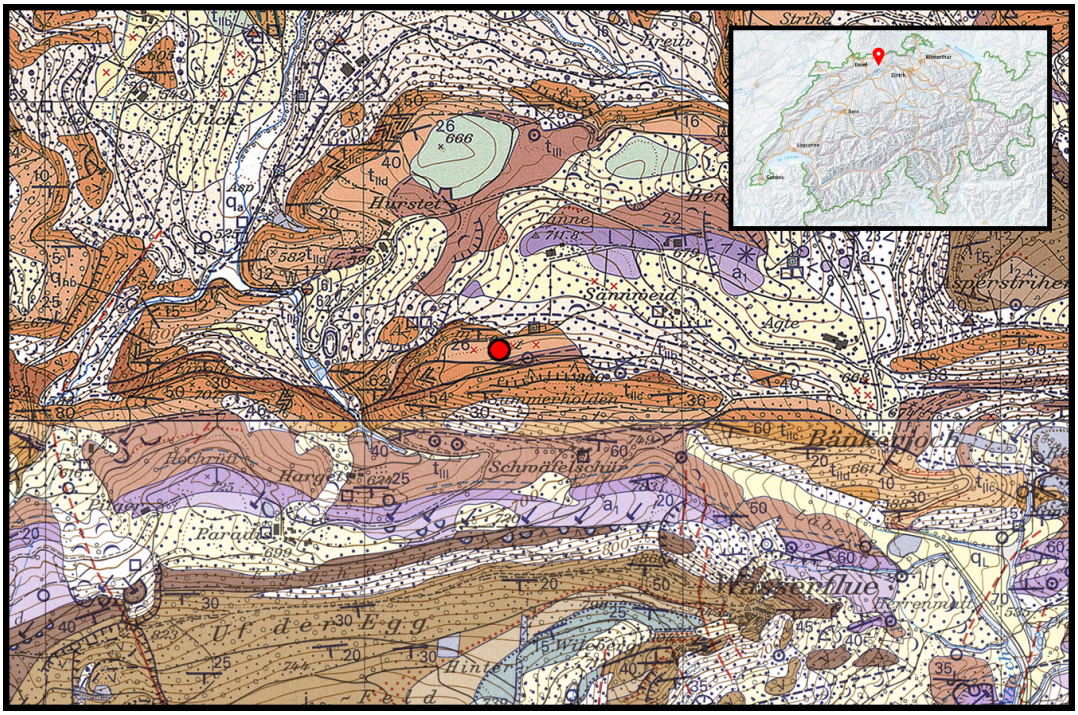

Figure 2 - *Geological map of the measuring area, in the surroundings of Emmethof (reproduced from Geological Atlas of Switzerland 1:25000, Swisstopo, modified). In red, the approximate location of the permanent station EMMET.*

From the geological points of view (**Figure 2**) the target area sits on outcropping calcareous (Muschelkalk) and dolomitic formations (Keuper) of Triassic age (t_{iid}-t_{iic}). Geological map shows that calcareous bedrock is in many areas exposed, but discontinuously covered by spots of Quaternary sediments. The region is nevertheless tectonically quite complex, with alternation of formation with different lithology over a relative short distance. By visual survey, the surface morphology is considerably smooth and modeled by the action of glaciers during the Pleistocene. Geophysical bedrock is never exposed at the measuring site, but likely very shallow. Such site can be classified as of rock ground-type A.

5. Acquisition equipment

Each acquisition point within the array consisted of a three components seismometer (Lennartz 3C with 5s eigenperiod) and a 24 bit data logger (Quanterra Q330). Synchronization between stations was assured by standard GPS, while a more accurate differential GPS (Leica Viva system) was used to precisely locate the sensor's coordinates with a tolerance of less than 5cm.

Figure 3 - *Overview of the measurement area during the acquisition of array configuration R1. SED station EMMET is located on the right side of the picture, close to the small path visible in background.*

6. Pre-processing and preliminary data-quality control

The three-component recording has been filtered prior to analysis using a band-pass 6th order causal Butterworth filter with corners at 0.2Hz and 50Hz. Although it is not a strict requirement for spectral analysis techniques, such filtering was applied in order to facilitate the preliminary visual inspection of the noise traces and to evaluate the coherency of the wave-field (**Figure 4**). Such procedure gives essential information for the subsequent interpretation of the f-k analysis results. In particular, it was observed an anomalous behavior of station EMT02, whose recordings were affected by large high-frequency transients of unknown origin during great part of the R1 acquisition. Surprisingly, no sign of these transients is visible on other traces.

To assess the quality of the ambient vibration recordings, spectral analysis was subsequently performed. Because of the stochastic nature of the ambient vibration wave-field, a statistical approach has to be used, such as the estimation of the power spectral density (*PSD*). This approach is useful to evaluate the average energy level of the recordings in the analyzed frequency range, and to access the presence of spurious spectral peaks, which might be related to human activity (machinery, pumps). By inspecting the PSD of all the three-component recordings of the array in the range between 0.5 and 40Hz, it is found that the average energy level of the spectrum fits well within the minimum and maximum bounds of the USGS noise model (**Figure 5**A), with a progressive increase of energy at high frequency, although no significant peaks of possibly anthropogenic origin are visible.

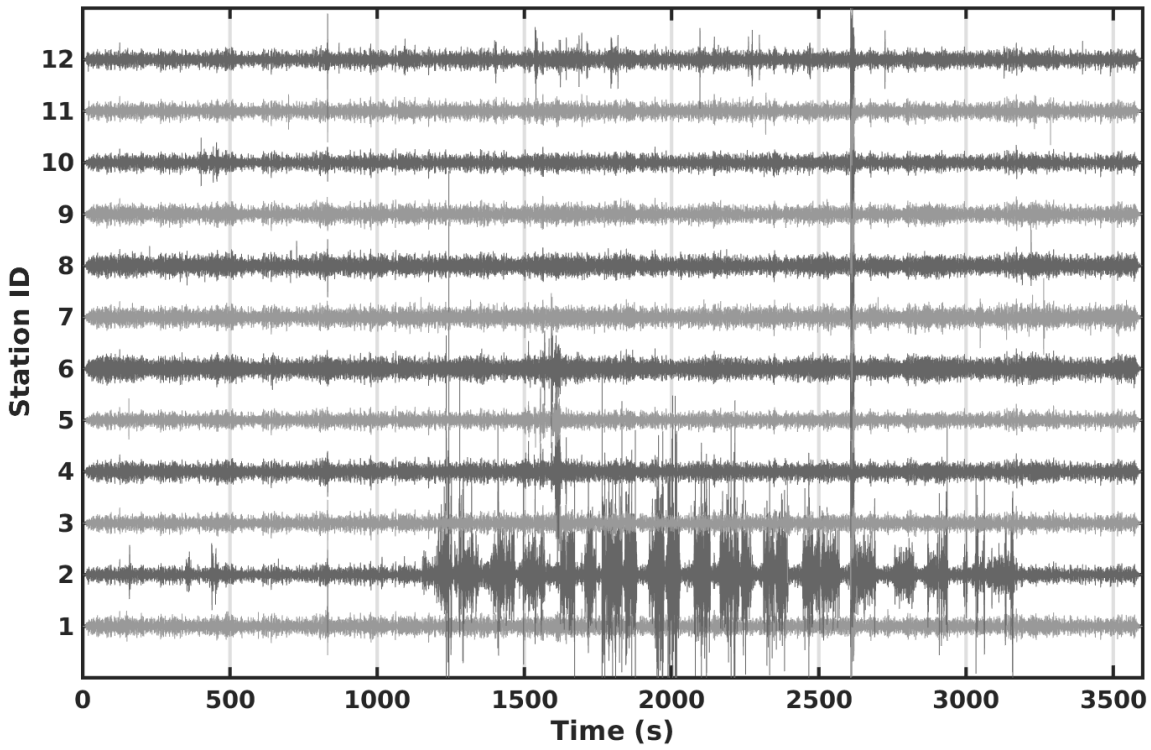

Figure 4 - *Inspection of the useful part of the ambient vibration recording of the Emmethof array (here configuration R1). A considerable amount of high-frequency transients of unknown origin affected station EMT02 during the acquisition, which was removed before subsequent f-k processing.*

Only for station EMT02, as previously mentioned, spectral analysis confirmed a contamination by rather high-frequency disturbances affecting all components (**Figure 5**B). The trace was therefore rejected from subsequent analysis.

Complementary to the aforementioned statistical methods, a spectral decomposition approach is more suitable to assess the stationarity of the ambient vibration wave-field over time. The wavelet time-frequency analysis was then performed over the whole recording time. From such analysis (**Figure 6**) an overall stability of the ambient-vibration wave-field over time is evident. No relevant harmonic signals can be identified in the frequency band useful for the processing, with the exception of few episodic contributions at very high-frequencies (>50 Hz), nevertheless discontinuous over the whole recordings and components. These contributions will not likely affect the following processing steps.

A) EMT01 (Central Station)

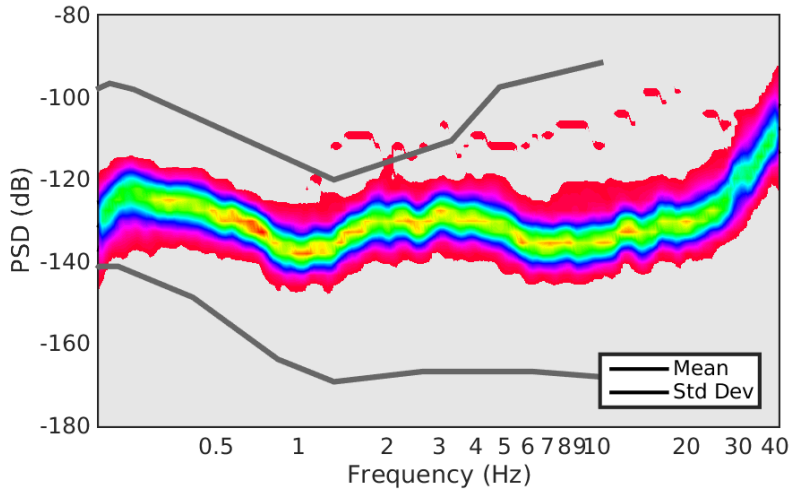

B) EMT02

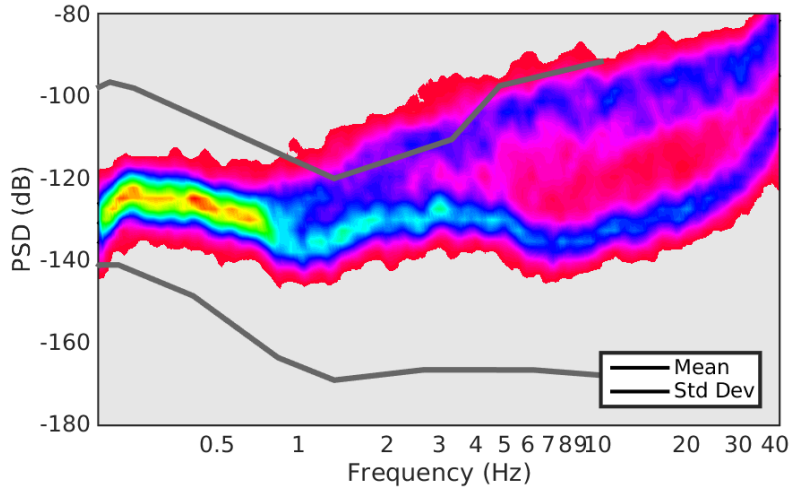

Figure 5 - *Power spectral density (PSD) computed for 1h recording at the central station of the array configuration R1 (EMT01, top) and at the station EMT02 (bottom). This last showed contamination of local high-frequency disturbances affecting the three components (in the plot horizontal direction N-S). Results similar to central station were nevertheless obtained for the other stations of the array. In gray lines are the minimum and the maximum bounds of the USGS noise model, for comparison.*

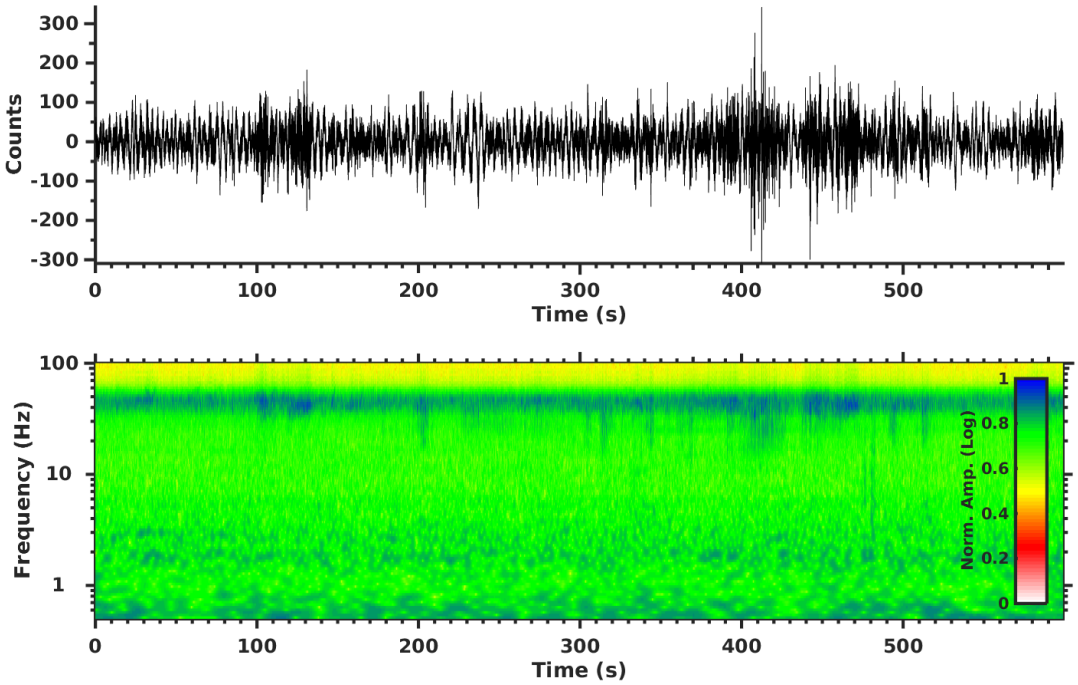

Figure 6 - *Example of spectrogram from 600s of recording of the central station (EMT01) of the array configuration R1, component N-S. No significant harmonic disturbances are visible on the whole spectrogram. Similar results were found for the other components. For the analysis, the cosine wavelet is used (wavelet parameter = 12).*

7. Conventional H/V spectral ratios

The horizontal-to-vertical (H/V) Fourier spectral ratio is a technique widely used in seismic site characterization because of its ability to provide an estimate of the SH wave fundamental frequency of resonance (f_0) of the site. Other than that, H/V ratios are useful to provide information on the Rayleigh wave ellipticity function, which can be used in surface wave dispersion inversion procedures to constrain large velocity contrasts at depth. In this study, we use the H/V technique also to map the variability of the subsoil structure along the investigated area; this is necessary to verify the fulfillment of the 1D structure assumption, which is necessary for the f-k method applied later.

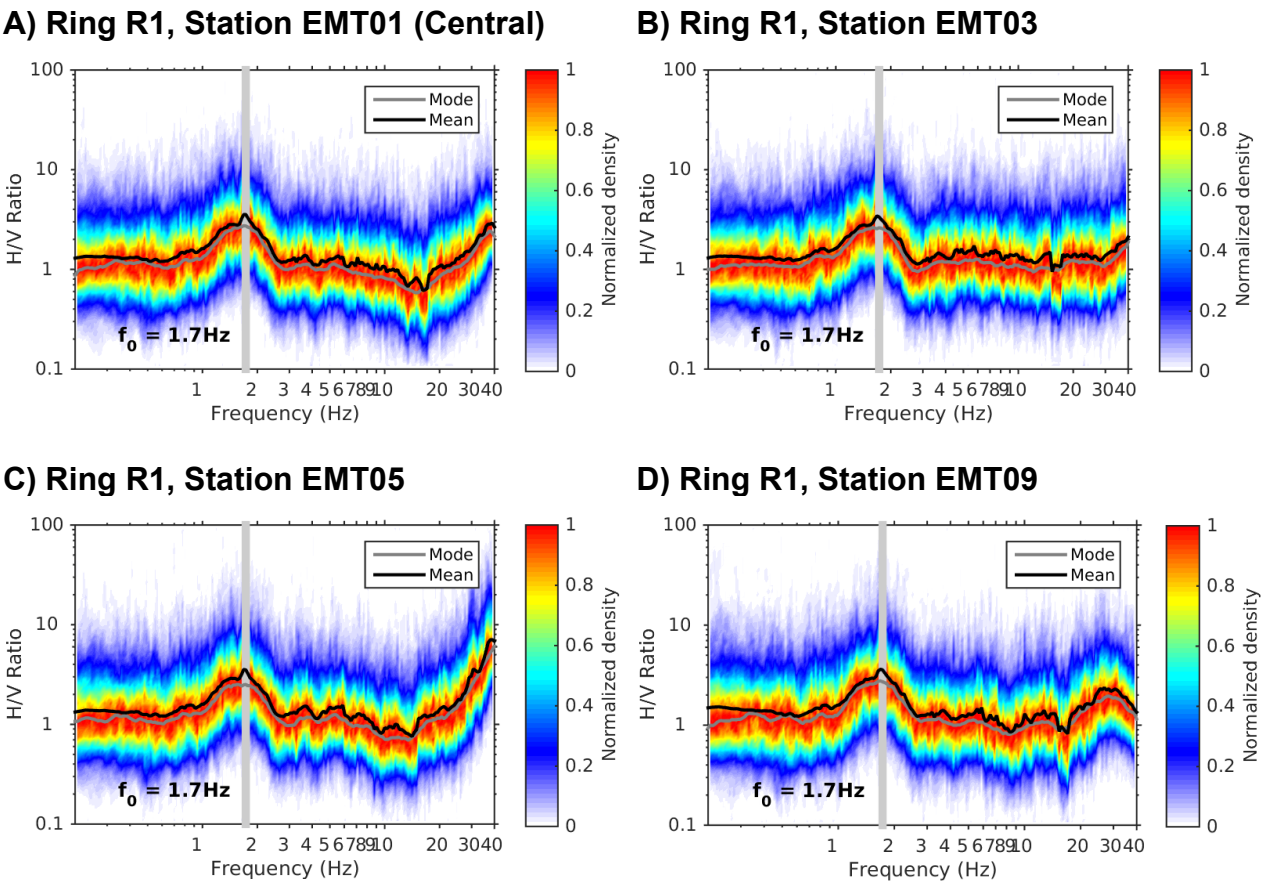

Figure 7 - *Example of H/V spectral ratios for the configurations R1. The resonance frequency of the cover is indicated with a light gray line (stable at 1.7Hz).*

H/V spectral ratios have been computed for all the recordings at each station of the array and separately for configurations R1 and R2 (e.g. **Figure 7**). The behavior of the noise wave-field at the different stations location is comparable at low to intermediate frequencies (roughly < 15Hz), while the high frequency region shows some variability, within and between array rings. This is likely due to variability of the top layers, which can show some heterogeneity over the measuring area. The behavior of the site can nevertheless be considered sufficiently homogeneous for the f-k analysis.

In average (**Figure 8**), spectral curves show a very stable low frequency peak at about 1.7Hz. Such maximum is likely induced by the presence of a deep interface, possibly between rocks of different competence. We assume such frequency peak to be the fundamental frequency of the site, later use as a constraint for the inversion of the deep portions of the velocity profile.

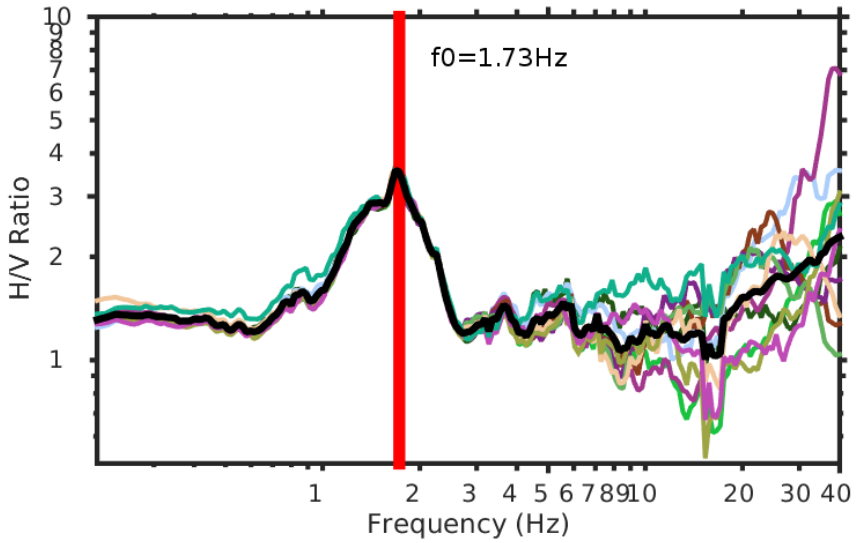

Figure 8 - *Comparison of the H/V spectral ratio curves of all the stations of the array (in this example for the array configuration R1). The curves are generally stable at low frequencies, confirming the lateral homogeneity of the underlying bedrock velocity structure. High frequencies (> 15Hz) show more variability, nevertheless in an acceptable range for the validation of one-dimensional assumption. The average fundamental peak of resonance is stable at about 1.7Hz.*

8. Directional analysis

The computation of directional H/V spectral ratio or polarization analysis is useful to reveal asymmetries in the ambient vibration wave-field. Different effects can induce such a behavior: 2D/3D structure, topographic effects or a non-homogeneous distribution of the noise sources. If a strong directionality is found by the analysis, it is generally recommended to carry out further investigations to properly address the origin of polarization. By processing the directional H/V ratios at all the recording stations of the two arrays (e.g. **Figure 9**) it is possible to observe an overall isotropy of the wave-field in the whole analyzed frequency range with the exception of the fundamental frequency peak (about 1.7 Hz), which shows a strong preferential alignment along NE-SW, stable between the different station locations of the array. Such behavior is of difficult interpretation; the hypothesis of dipping layer should be rejected by the confirmed stability of the resonance peak at the different measuring places. Topography features have no apparent relation with such directionality. The possibility of anisotropic noise source distribution will be later discussed in light of f-k analysis results.

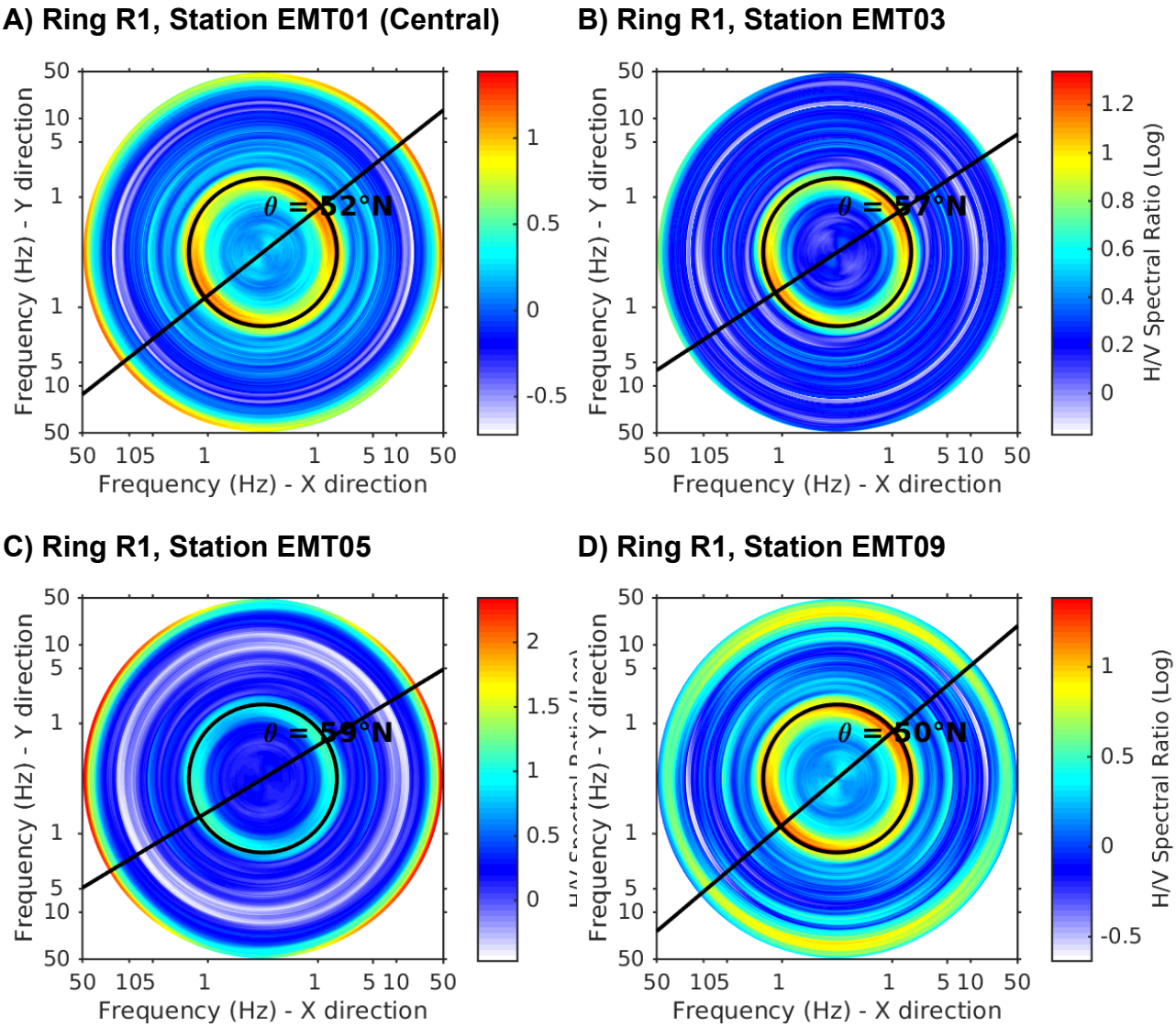

Figure 9 - *Example of directional H/V spectral ratios for configuration R1. A strong preferential direction of the resonance peak is present, roughly aligned NE-SW. However, other frequency bands show a more isotropic behavior of the noise wave-field.*

The results of the H/V directional analysis are confirmed by applying the wavelet polarization analysis technique (Burjanek et al., 2008). Here, the particle motion shows to be mostly elliptical, with a significant polarization only at the resonance frequency (**Figure 10**). As well, resonance frequency is associated with a mild azimuthal anisotropy, in agreement with previous H/V results (**Figure 11**A).

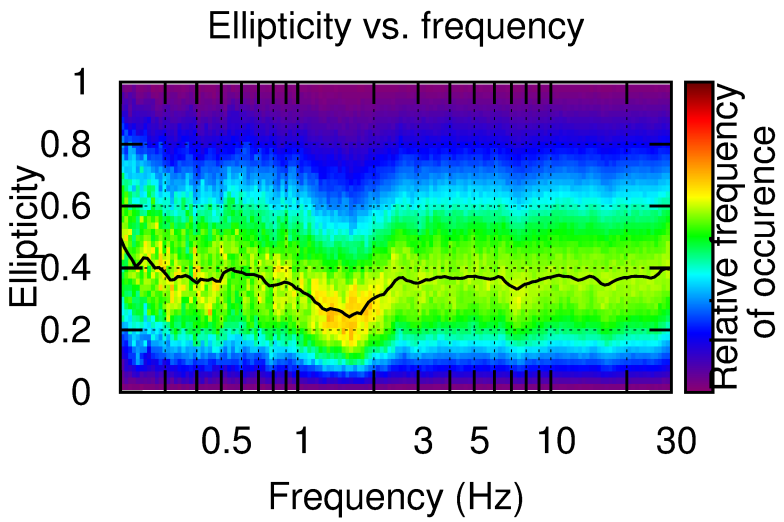

Figure 10 - *Ellipticity of the particle motion from wavelet-based polarization analysis at the central station of the array (EMT01). Similar results can be obtained for other stations of the arrays.*

9. Three-component f-k analysis

The frequency-wavenumber analysis is a spectral technique based on seismic array recordings that allows retrieving direction and dispersion characteristics of the surface waves. We apply this technique to three-component ambient vibration recordings using a modification of the high-resolution method of Capon (1969) as described in Poggi et al. (2010). Using all the three-components of motion gives the possibility to retrieve information about the propagation of the Rayleigh waves (vertical and radial processing direction) as well as of the Love waves (transversal direction). As in the case of the previous methods, the ambient vibration recordings are treated statistically by subdividing the traces in sub-windows. For each consecutive window, a separated f-k analysis is performed, and the results are then averaged over the whole recording, increasing the robustness of the final estimation.

As first step, from the f-k analysis it is possible to assess the azimuthal distribution of noise sources over different frequency ranges (e.g. **Figure 12**) separately for the vertical, the radial and the transversal direction of polarization. From the analysis of the two geometries R1 and R2, source distribution appears to be quite homogeneous for all the components, without displaying a clear directional pattern. Unfortunately, resolution limits of the two configurations do not allow investigating the source distribution at low frequencies (in particular at f_0), which would have been essential to understand the directionality pattern observed in H/V and polarization analysis.

A)

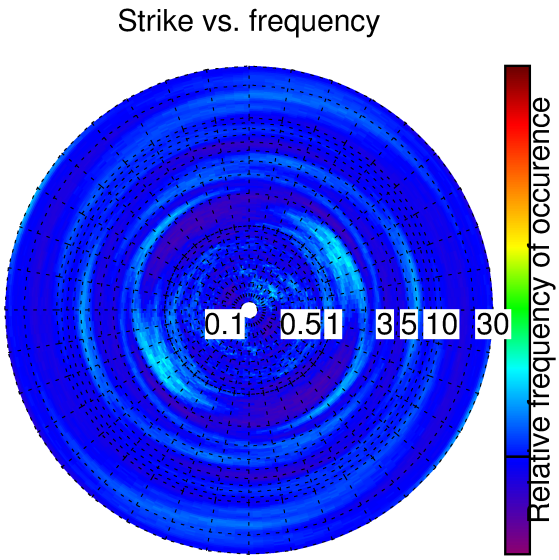

B)

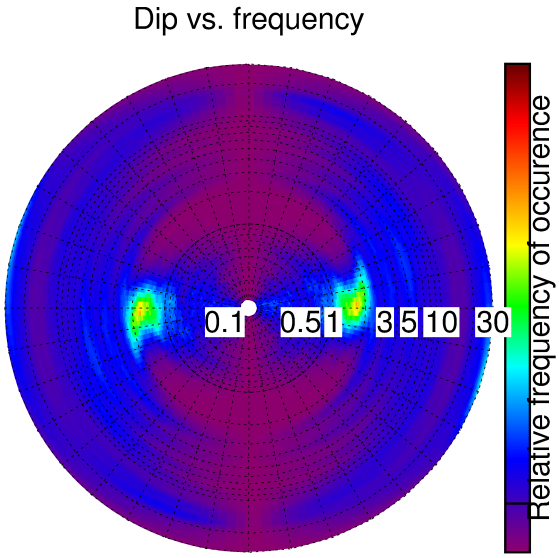

Figure 11 - *Directionality of the particle motion from wavelet-based polarization analysis (dip direction in A, strike in B) at the central station of the array (EMT01). Similar results can be obtained for other stations of the arrays.*

A) Ring 1, 12-20Hz

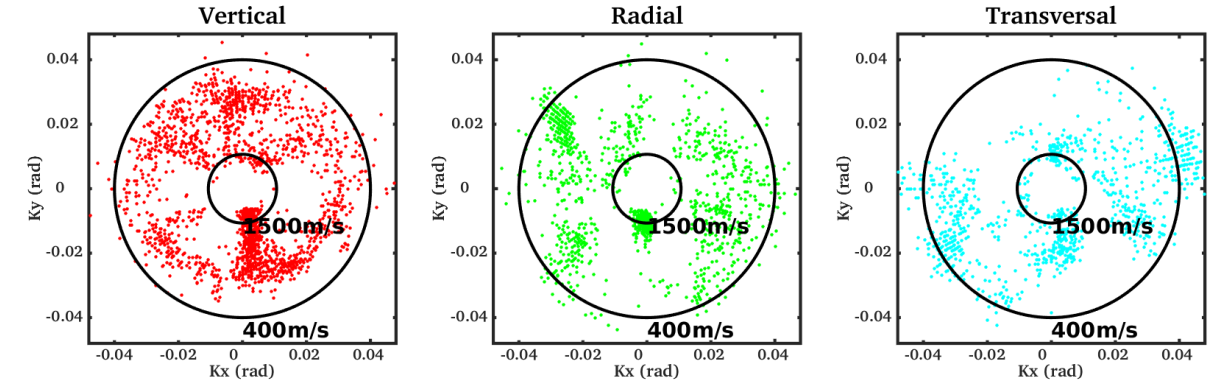

B) Ring1, 20-30Hz

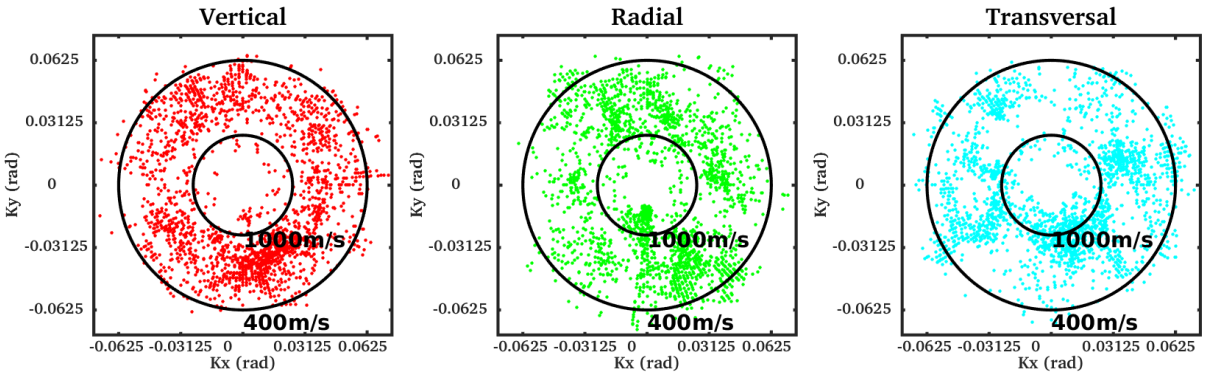

Figure 12 - *Example of distribution of noise sources in the intermediate (12-20Hz) and high frequency range (20-30Hz) obtained from three-component f-k analysis. The source distribution is irregular but not strictly directional on all the propagation components.*

As a second step, the surface-wave dispersion curves are extracted by visual inspection and manual picking of the f-k density plots (**Figure 13**), separately for the three polarization directions. Good results are obtained for the array configuration R1, while R2 did not show usable evidence of dispersion in the resolved frequency band. Given the high velocity of the site, results from R1 are nevertheless sufficient to provide a reasonable constraint for the inversion of the velocity profile of the site.

More in detail, Love wave's fundamental mode dispersion can be well tracked in the frequency range between about 18Hz and 35Hz. The Rayleigh wave's fundamental mode is also clearly visible on the vertical component of R1, between 12Hz and 40Hz, but of more problematic identification on the radial direction. The final interpretation of Rayleigh and Love wave dispersion pattern is given in **Figure 14**.

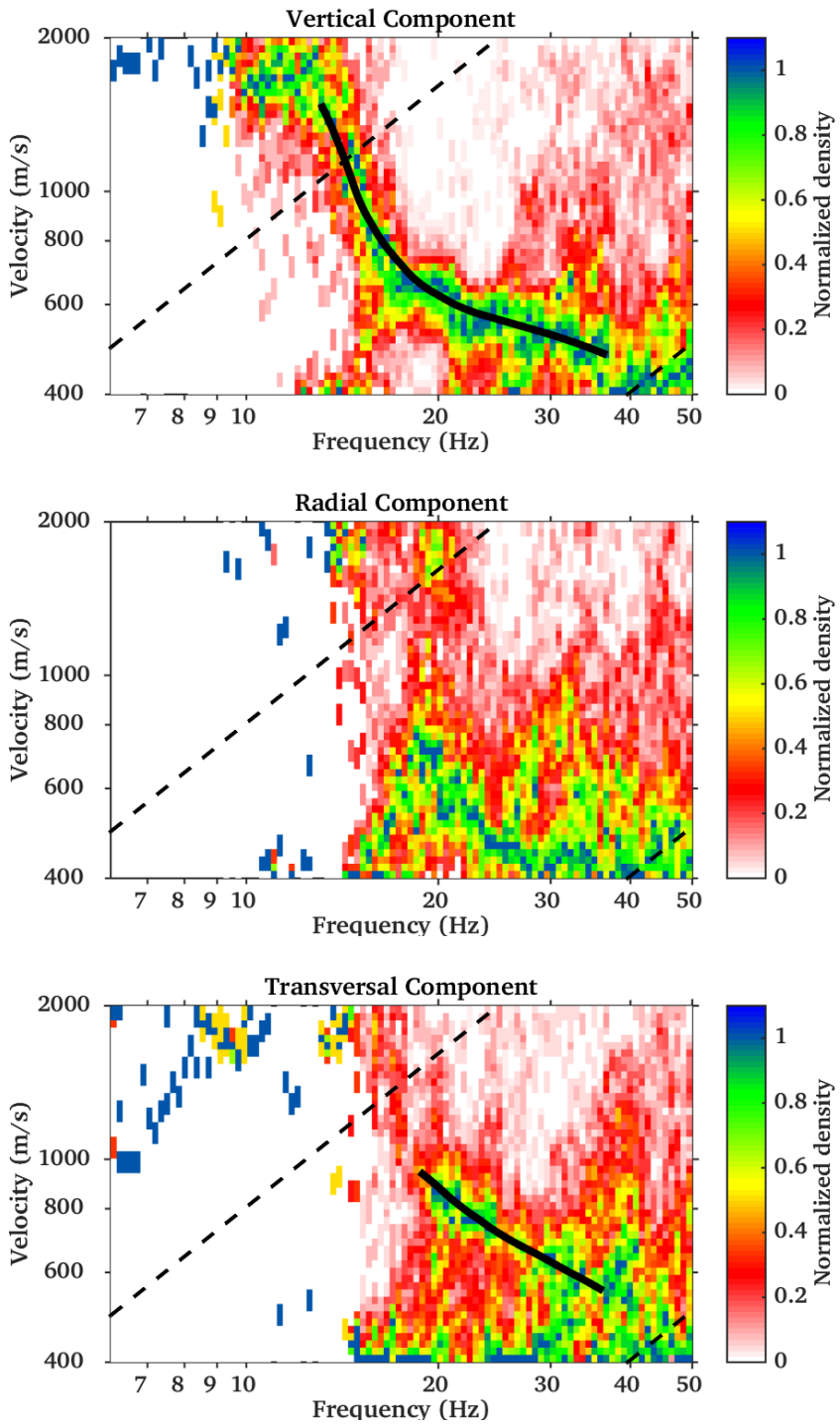

Figure 13 - *Density distribution of the surface wave signals obtained from the recording of the array configuration R1 using three-component f-k analysis. From top to bottom: Rayleigh vertical, Rayleigh radial and Love wave dispersion. In black, the interpreted dispersion curves are given (manually selected).*

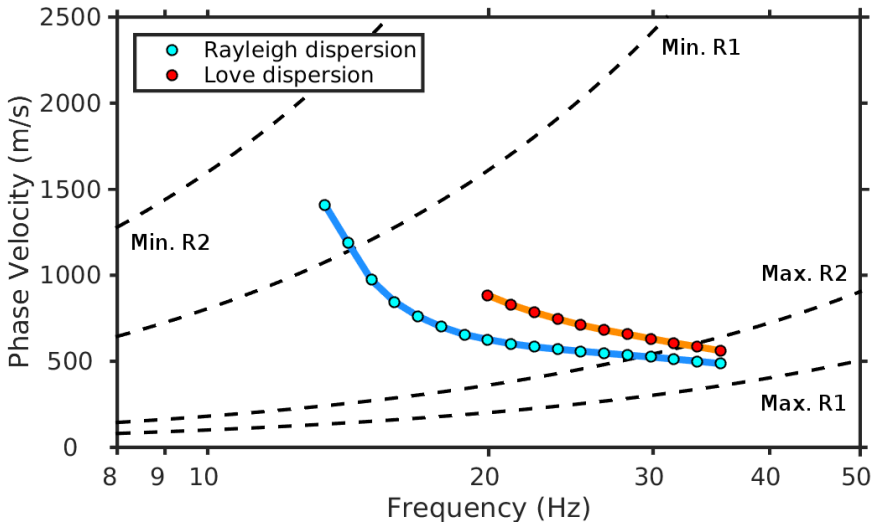

Figure 14 - *Summary of all dispersion curves obtained from three-component f-k analysis of the array configuration R1. Minimum and maximum resolution bounds from the two geometries are indicated with black dashed lines for comparison.*

10. Inversion of the dispersion curves

The surface wave dispersion curves (Rayleigh and Love) obtained from the three-component f-k analysis of the ambient vibrations and the fundamental frequency of resonance (f_0) from average H/V spectral ratios are inverted to obtain an estimation of the velocity profile of the site (mainly S-wave velocity as function of depth, and to a lesser extend the P-wave velocity, due to the lower sensitivity). The analysis is performed using the software *Dinver* (www.geopsy.org), which implements a direct search approach (**Figure 15**) based on a conditional version of the neighborhood algorithm (Sambridge, 1999).

To parameterize the velocity model, two different approaches were implemented. The first one consisted in setting up an eight-layer model with fix interface depths. In such a case, the free inversion parameters are then the velocities (P and S) and layer thicknesses. In the second case, a free-thickness layer approach was used. The advantage of the former method stays in the possibility to better resolve sharp velocity interfaces, while the second is less unique and better constraints the seismic velocity. The two approaches have to be nevertheless considered complementary, and they should provide consistent results.

Ten inversion tests (*runs*) were performed for each of the two model schemes, in order to minimize the effect related to a possible unfavorable initial randomization of the parameter space. The best fitting model from of each run was then collected (**Figure 16** and **Figure 19**) and used later on for the computation of the derived soil parameters.

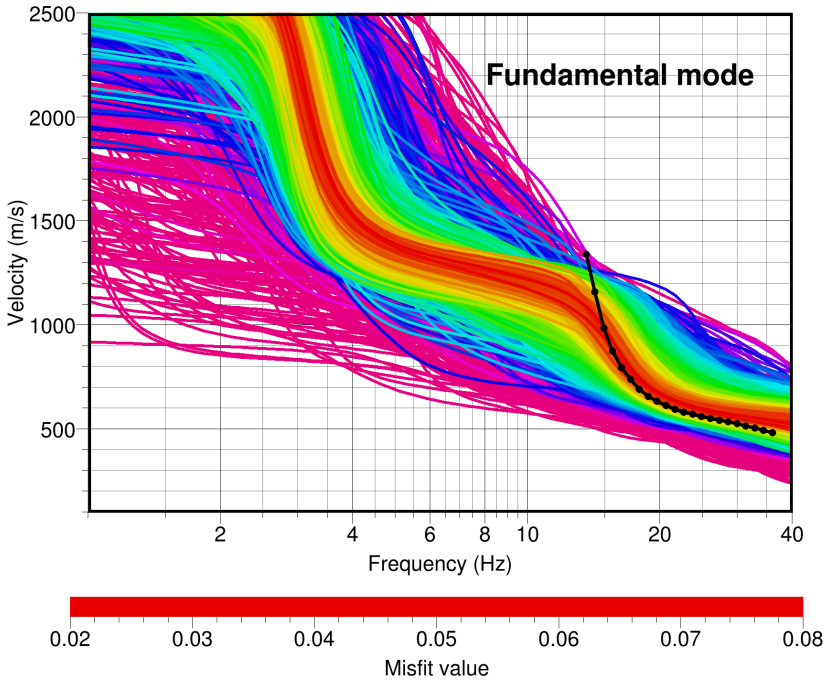

A)

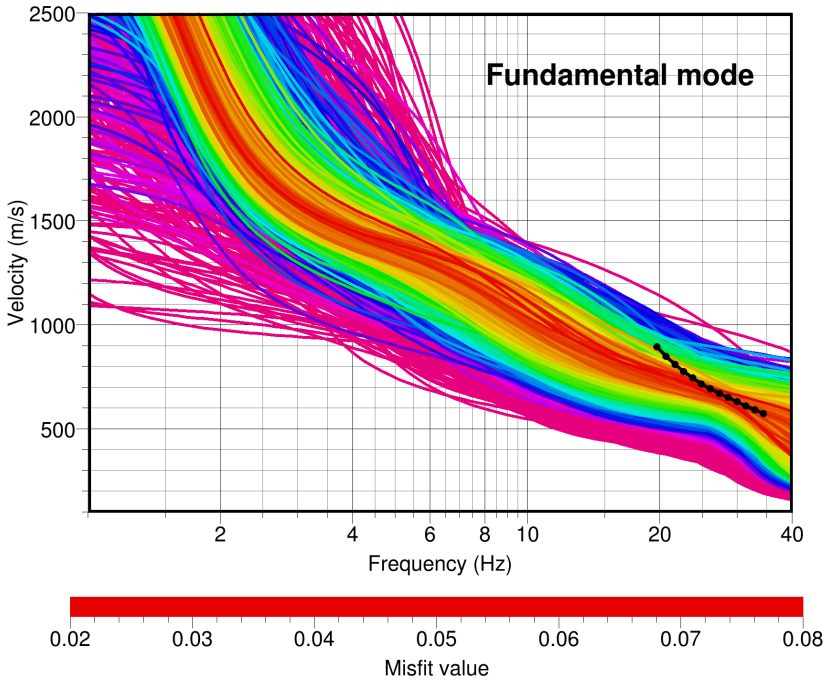

B)

Figure 15 - *Example of fitting the surface dispersion data within the global optimization procedure. Different colors represent different misfit between the observed (in black) and the modeled dispersion curves during the search (A, Rayleigh; B, Love).*

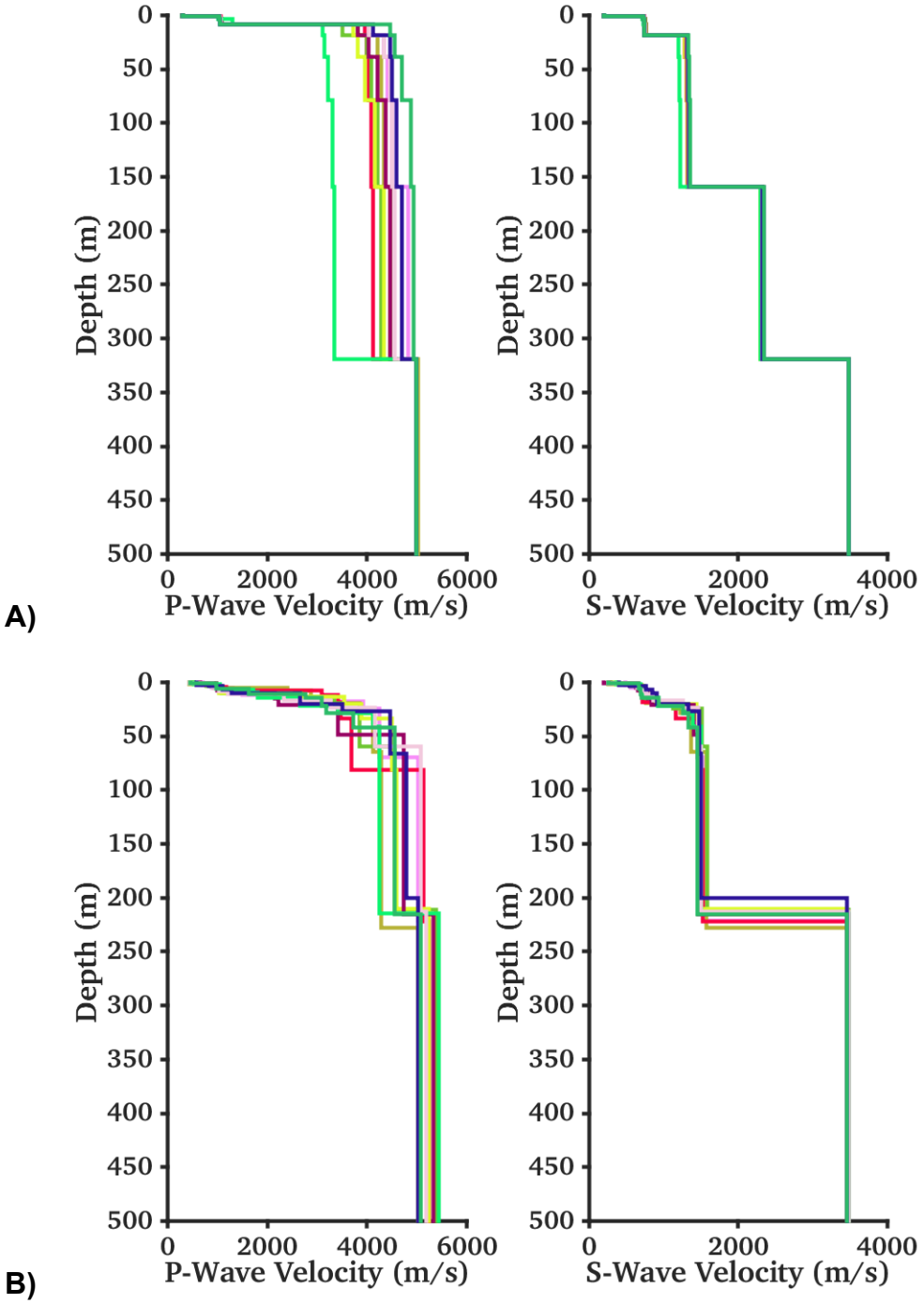

Figure 16 - *Collecting the best fitting models from the ten separated inversion runs using the free-layers (A, top) and fixed-layers (B, bottom) parameterization schemes.*

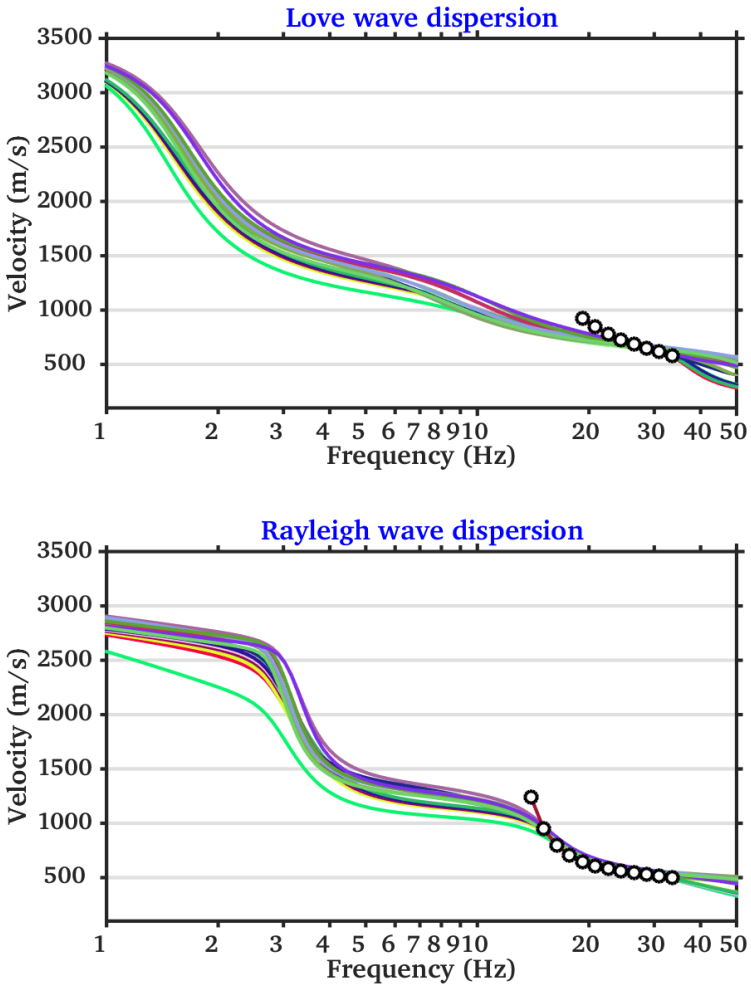

Figure 17 – *Rayleigh and Love dispersion curves computed from the 20 best fitting models of the two proposed interpretation schemes (free and fix layers).*

In more detail, the inverted velocity models (Vs and Vp) are gradient-like, with a faster increase in velocity in the first 100m, followed by a more regular part of nearly constant velocity. The large velocity contrast at about 200m (in the free layer approach) is constrained by the combined inversion with f_0 and the Rayleigh wave ellipticity right flank obtained from H/V spectral ratios (**Figure 18**). It is nevertheless interesting to notice that theoretical ellipticity match quite well the whole average H/V function, also at rather high frequencies.

By considering the minimum available frequency of the input data and by analyzing the scattering of the inverted models (**Figure 19**), it is realistic to assume the velocity profiles to be reliable down to a depth of about ~250m. Below this value no direct constrain is available from data, and the velocity values are obtained by pure extrapolation.

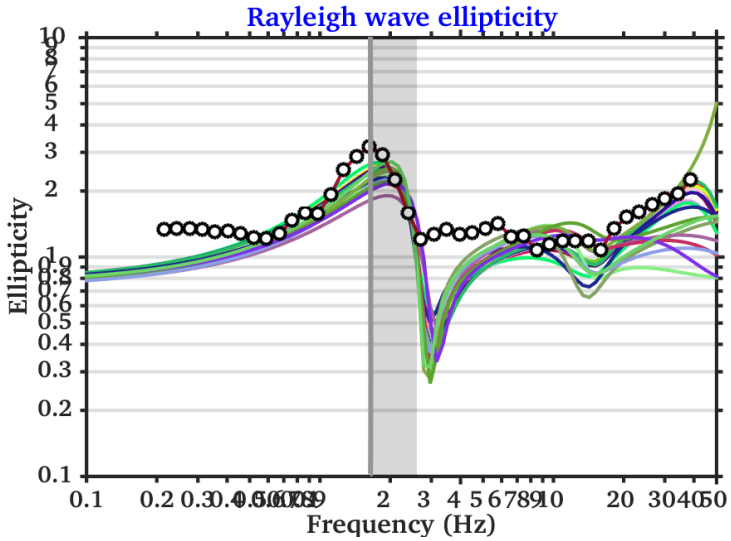

Figure 18 - *Rayleigh wave ellipticity curves computed from the best fitting models of the two proposed interpretation schemes (free and fixed layers), compared with average H/V spectral ratio from configuration R1 (scaled by sqrt(2)). Only the low frequency maximum (f_0) and the related right flank were used during the inversion.*

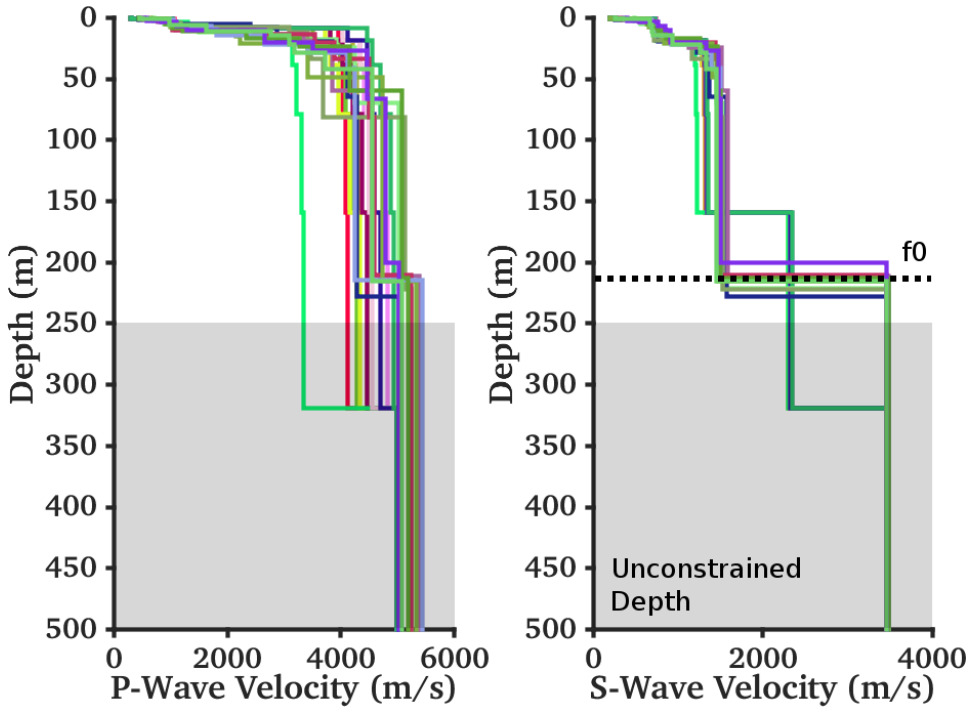

Figure 19 - *Comparison of all the best models from the two parameterization schemes (free and fixed layers). The two approaches produce consistent results. The depth of about 250m is considered approximately the maximum resolved depth.*

11. Engineering soil parameters

The ensemble of all the best inverted velocity profiles is then used to derive average soil parameters like the VsZ (average travel-time S-wave velocity over the depth Z, including Vs30, Table 1) and the quarter-wavelength (QWL) average velocities (Joyner et al., 1984) for a range of frequencies between 0.6 and 30Hz (**Figure 20**). The former is a standard parameter for the classification of ground-types in most building codes and in ground motion prediction equations. The latter is a parameter useful for the empirical estimation of the site-response and to assess the sensitivity of the seismic wave-field to the different depths. It has to be noticed that these two parameters are derived separately from all the best S-wave velocity models obtained from the inversion, and the results is finally averaged to improve statistics.

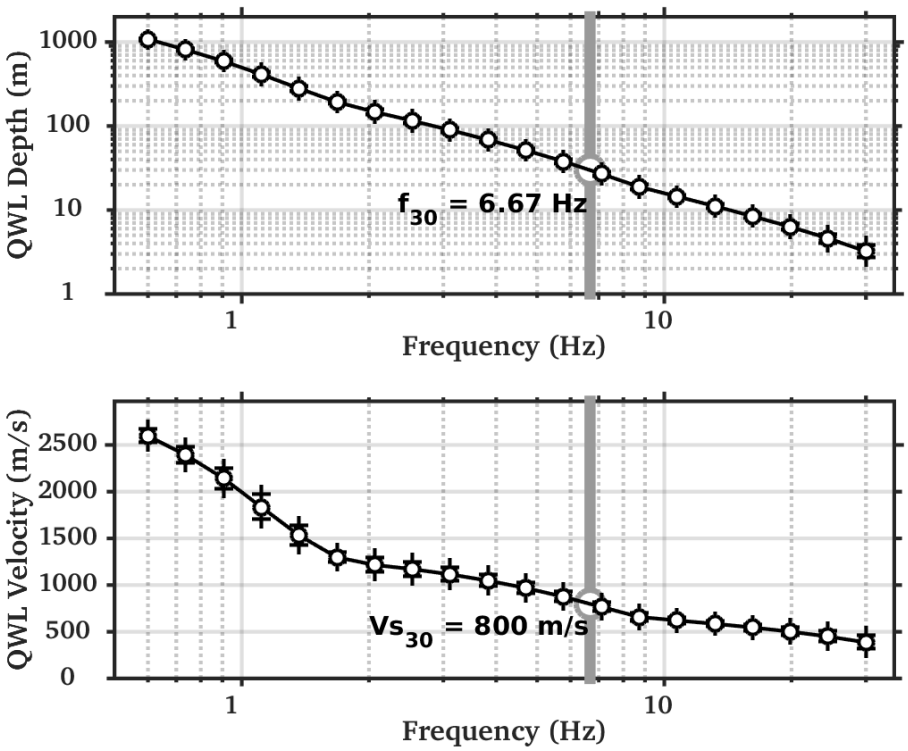

Figure 20 - *Quarter-wavelength representation of the inverted S-wave velocity profiles. Top: the depth-frequency dependency. Bottom: the QWL average velocity. The Vs30 value is indicated with its corresponding QWL frequency.*

Averaging depth (m)	Vs-mean (m/s)	St.Dev.
5.00	468.12	36.01
10.00	571.58	24.65
15.00	625.89	26.81
20.00	672.68	28.93
25.00	741.49	27.91
30.00	800.73	31.30
40.00	892.53	36.96
50.00	960.55	41.12
75.00	1071.72	50.56
100.00	1140.80	58.26
150.00	1220.08	68.98
200.00	1316.13	32.38

Table 1 - *Average travel-time velocities at different depths. Vs30 is highlighted.*

12. Amplification models

Site amplification functions have been computed using two different approaches: the S-wave transfer function for vertical propagation and the quarter-wavelength amplification. In general the first method is used to evaluate the resonance characteristics of the site, while the second is more useful to assess the effect of the velocity contrasts between the lowermost rock layer (as reference) and the different QWL averaging depths. The two amplification functions are then corrected for the Swiss rock reference velocity profile as defined in Poggi et al. (2011), according to the procedure described in Edwards et al. (2013). Given the lower velocities in the uppermost part of the EMMET profile compared to the Swiss reference, the final corrected amplification function shows a lower average amplification level at high frequencies than the uncorrected (**Figure 21**), while low frequency part is nearly asymptotic.

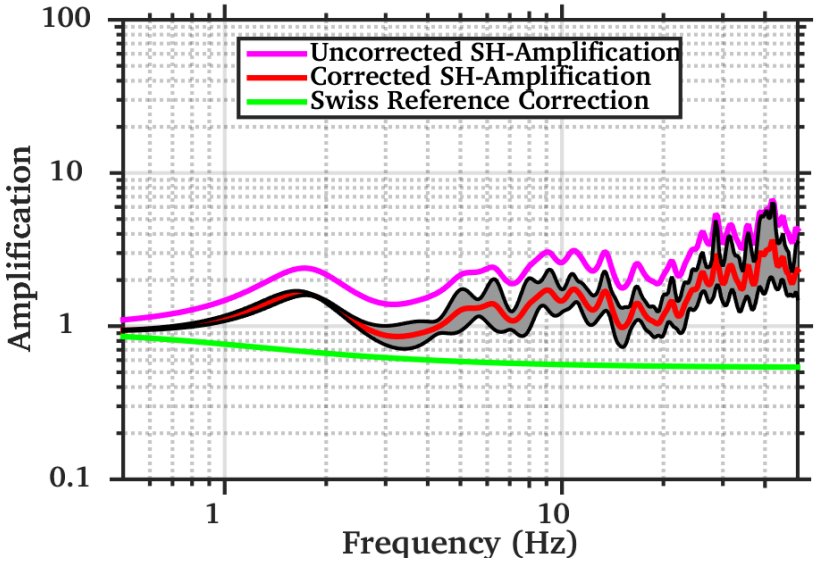

Figure 21 - *Correcting the SH-wave transfer function for the Swiss (rock) reference conditions (Poggi et al. 2011). The final corrected amplification function shows a lower (average) amplification at high frequencies than the uncorrected.*

Amplification functions using the transfer function and the quarter-wavelength approach are comparable (**Figure 22**), even if the transfer function provides a slightly larger amplification, because of the presence of some weak resonance peaks. At low frequencies both methods converge to the same average amplification level. It has to be notice that the amplification functions do not include attenuation at this stage of the analysis, as the quality factors of the site are too uncertain.

A good matching is obtained by comparison between the one-dimensional transfer function and the empirical amplification from spectral modeling of low-magnitude earthquakes as described in Edwards et al., 2013 (**Figure 23**). Resonance peaks are mostly well reproduces by analytical solution, even though empirical amplification presents a minor positive offset at low frequency, which cannot be explained by the available data.

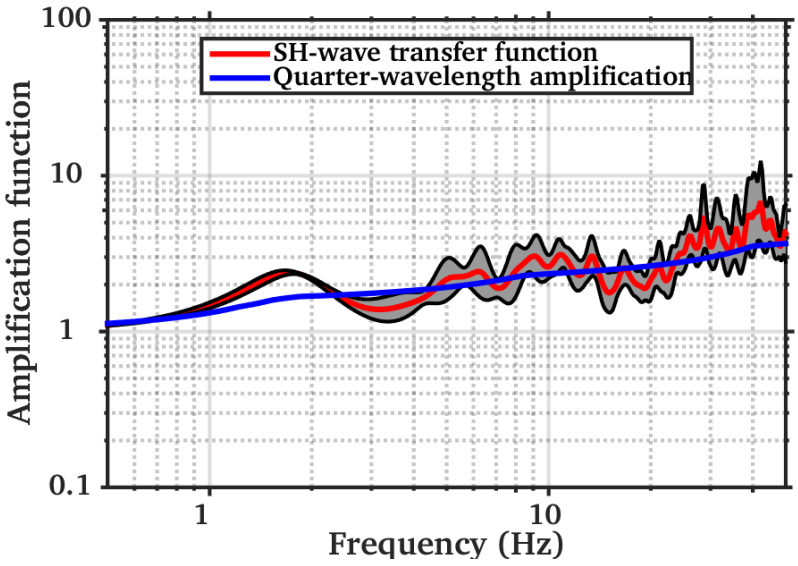

Figure 22 - *Comparison of amplification functions computed using the SH-wave transfer function and the quarter-wavelength formalism on the inverted velocity models.*

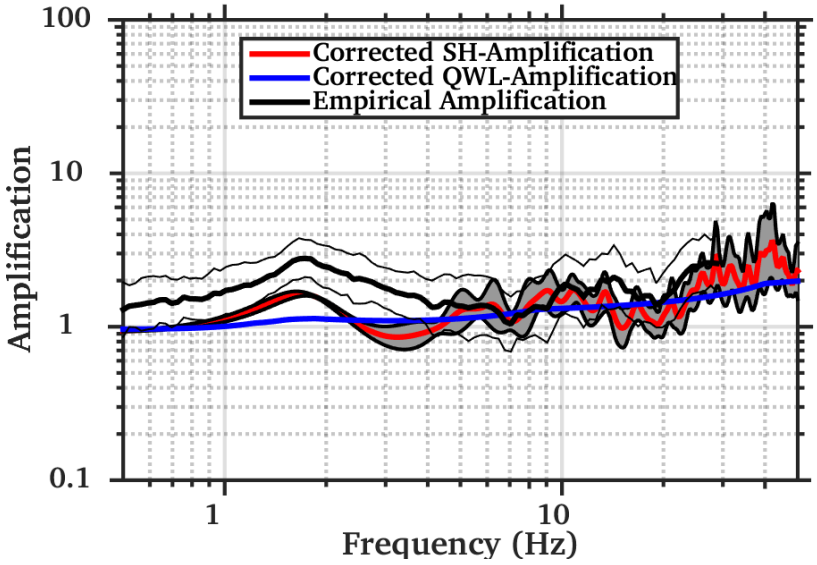

Figure 23 - *Comparison of amplification functions computed using the SH-wave transfer function and the quarter-wavelength approach with empirical observation from spectral modeling of low-magnitude earthquakes. All functions are referenced to the Swiss rock reference model (Poggi et al. 2011).*

REFERENCES

Capon, J., 1969. High resolution frequency wavenumber spectrum analysis, Proc. IEEE, 57, 1408-1418.

Burjanek, J., G. Stamm, V. Poggi, J.R. Moore, and D. Fäh [2010], "Ambient vibration analysis of an unstable mountain slope", Geophys. J. Int., Vol. 180, pp. 820-828.

Edwards, B., C. Michel, V. Poggi and D. Fäh (2013). Determination of Site Amplification from Regional Seismicity: Application to the Swiss National Seismic Networks. Accepted for publication in Seismological Research Letters.

Joyner, W. B., R. E. Warrick and T. E. Fumal (1981). The Effect of Quaternary Alluvium on Strong Ground Motion in the Coyote Lake, California, Earthquake of 1979, Bulletin of the Seismological Society of America, 71, 1333-1349.

Poggi, V., B. Edwards and D. Fäh (2011). Derivation of a Reference Shear-Wave Velocity Model from Empirical Site Amplification, Bulletin of the Seismological Society of America, 101, 258-274.

Poggi, V. and Fäh D., 2010. Estimating Rayleigh wave particle motion from three-component array analysis of ambient vibrations. Geophys. J. Int., 180-1, 251-267.